HHS Public Access

Author manuscript

J Immunol. Author manuscript; available in PMC 2024 July 01.

Published in final edited form as:

J Immunol. 2023 July 01; 211(1): 23–33. doi:10.4049/jimmunol.2200949.

Mutations to the BTN2A1 linker region impact its homodimerization and its cytoplasmic interaction with phosphoantigen-bound BTN3A1

Khiem Nguyen[*], **Yiming Jin**[*], **Matthew Howell**[†], **Chia-Hung Christine Hsiao**[*], **Andrew J. Wiemer**[*,‡], **Olga Vinogradova**[*]

[*]Department of Pharmaceutical Sciences, University of Connecticut, Storrs, Connecticut, 06269

[†]Department of Chemistry, University of Connecticut, Storrs, Connecticut, 06269

[‡]Institute for Systems Genomics, University of Connecticut, Storrs, Connecticut, 06269

Abstract

Intracellular binding of small molecule phosphoantigens to the HMBPP receptor complex in infected cells leads to extracellular detection by T cells expressing the Vγ9Vδ2 T cell receptor, a non-canonical method of antigen detection. The butyrophilin proteins BTN2A1 and BTN3A1 are part of the complex, however, their precise roles are unclear. We suspected that BTN2A1 and BTN3A1 form a tetrameric (dimer of dimers) structure and we wanted to probe the importance of the BTN2A1 homodimer. We analyzed mutations to human BTN2A1, utilizing internal domain or full length BTN2A1 constructs, expressed in *Escherichia Coli* or human K562 cells, that might disrupt its structure and/or function. Though BTN2A1 is a disulfide-linked homodimer, mutation of cysteine residues C247 and C265 did not affect the ability to stimulate T cell interferon γ production by ELISA. Two mutations of the juxtamembrane region (at EKE282) failed to impact BTN2A1 function. In contrast, single point mutations (L318G and L325G) near the BTN2A1 B30.2 domain blocked phosphoantigen response. SEC and NMR experiments showed that the isolated BTN2A1 B30.2 domain is a homodimer, even in the absence of its extracellular and TM region. ^{31}P-NMR experiments confirmed that HMBPP binds to BTN3A1 but not BTN2A1, and binding abrogates signals from both phosphorus atoms. Furthermore, the BTN2A1 L325G mutation but not the L318G mutation prevents both homodimerization of BTN2A1 internal domain constructs in SEC (and NMR) experiments and their binding to HMBPP-bound BTN3A1 in ITC experiments. Together, these findings support the importance of homodimerization within the BTN2A1 internal domain for phosphoantigen detection.

Introduction

Our immune response is a vital component to our health due to its involvement in detection and removal of harmful entities. T cells, in particular, are involved in the recognition of antigens, which are usually peptides presented by major histocompatibility complexes (MHC). However, some T cells contain less variable T cell receptors which can be used

Correspondence: Phone Number: 860-486-3966 (AW), 860-486-2972 (OV), Fax Number: 860-486-6857, andrew.wiemer@uconn.edu, olga.vinogradova@uconn.edu.

for detection of non-peptide antigens. A subset of γδ T cells, the Vγ9Vδ2 T cells, have garnered particular attention because they can be activated independent of MHCs through detection of small-molecule phosphoantigens (pAgs) (1, 2) such as (*E*)-4-hydroxy-3-methyl-but-2-enyl diphosphate (HMBPP), a bacterial intermediate of lipid synthesis. Elucidating the signaling pathway of pAg-dependent activation would provide a better understanding of the immune system while offering potential insights for future therapeutics, such as anti-tumor immunotherapies that work through γδ T cell activation (3, 4).

It has been established that in antigen presenting cells the pAgs can directly bind to the cytoplasmic B30.2 domain of butyrophilin 3A1 (BTN3A1), a transmembrane protein belonging to the immunoglobulin superfamily (5–10). This interaction results in a conformational change within BTN3A1 (7, 11–13), impacts its clustering and leads to the activation of Vγ9Vδ2 T cells. Though the initial hypothesis was that recognition would involve Vγ9Vδ2 T cell receptors directly binding to BTN3A1, this has not been supported by experimental data, suggesting that additional factors are necessary. These additional factors are now realized to include the other BTN3A isoforms BTN3A2 and BTN3A3.

More excitingly, recent data has implicated the involvement of a closely related isoform, BTN2A1 (14–17), where knockdowns of BTN2A1 hinder the activation of Vγ9Vδ2 T cells by BTN3A1 ligands (17). This is intriguing as there is evidence that BTN2A1 directly associates with Vγ9 TCR (14, 15, 18), meaning that BTN2A1 could potentially be the bridge required for BTN3A1 and T cell activation. This is complemented by further evidence that has shown that BTN3A1 and BTN2A1 can form a complex through colocalization and *in vitro* binding studies, where direct association of BTN2A1 to BTN3A1 requires pAg present (17).

Evidence is beginning to emerge supporting the organization of the BTN3A1/2A1 complex (or HMBPP receptor). However, the finer molecular details of complex formation leading to T cell recognition are not well understood. At a minimum, one molecule of BTN2A1 is required for binding the TCR, one molecule of BTN3A1 is required for binding the pAg, and one molecule of BTN3A2 is required for maximum response. Some have hypothesized that BTN2A1 and BTN3A1 form a heterodimer, but this unlikely given that it would exclude a role for BTN3A2. Furthermore, BTN2A1, but not BTN3A1, contain cysteine residues at positions where disulfide bonds can occur. Therefore, our preferred model for the active complex structure is that of a dimer of dimers (i.e. a tetramer) (Figure 1). In this paper, we further explore the dimerization of BTN2A1 and its impact on the binding interface between the BTN2A1 homodimer and pAg-bound BTN3A1. Through enzyme-linked immunosorbent assays (ELISA), isothermal titration calorimetry (ITC), nuclear magnetic resonance (NMR), and size exclusion chromatography (SEC), we demonstrate that the mutation BTN2A1 L325G reduces pAg detection, perturbs BTN2A1 binding to BTN3A1, and disrupts the homodimerization of the BTN2A1 internal domain. Together, this supports a model in which BTN2A1 homodimerization, particularly within the intracellular domain, is vital for BTN3A1-mediated pAg detection.

Methods

Reagents and supplies

Buffy coat was obtained from Research Blood Components. K562 cells were from Millipore Sigma. Lymphocyte separation media was from Corning. Human IL-2 and the TCRγ/δ+T cell isolation kit were from Miltenyi. HMBPP was from Cayman Chemical. POM_2-C-HMBP was from Prof. David Wiemer at the University of Iowa (7, 19). Unlabeled anti-his tag antibody (J095G46), PE anti-his tag antibody (J095G46) and ELISA kits for TNFα and IFNγ were from Biolegend. Rabbit anti-myc tag (#2272S) and mouse anti-myc tag (#2276) antibodies were from Cell Signaling. PCR primers were from IDT. BCA assay and Protein G agarose were from Pierce.

Generation of BTN2A1 constructs and mutants for cellular assays

We previously described cloning of full length BTN2A1 containing a C-terminal Myc tag (BTN2A1-myc) or an N-terminal 6x His tag (6xHis-BTN2A1) into pcDNA3.1 (+), as well as the mut1, mut2, L318G, W320A, and L325G mutations on both templates (17). Here, site directed mutagenesis was performed with the following primers: C247A-F, 5'- GCT GCA GTG GCC CTG CCT - 3'; C247A-R 5' – GGG AGA CAC ACT GGG CAT - 3'; C265A-F, 5' – GCC ATC TAT TGG ATC AAC AAA CTC – 3'; C265A-R, 5' – TAC GGC AAT GGG TAT CAT CA – 3'; EKE282AAA-F, 5' - GCC GCT GCT TTT GAA CGG GAA ACA AGA GAA – 3'; EKE282KKK-F, 5' – AAG AAG AAG TTT GAA CGG GAA ACA AGA GAA – 3'; EKE282-R, 5' – CCC TGA CAG AAT CTT TTT TTC CT - 3'. The primers were used to amplify the full plasmid, following which the template was digested with DpnI. The PCR product was phosphorylated with T4 kinase, ligated with T4 ligase, and transformed into DH5α cells. Single clones were validated by Sanger sequencing. This produced the C247A, C265A, C247A/C265A, EKE282AAA, and EKE282KKK mutations on the 6xHis-BTN2A1 construct in the pcDNA3.1 (+) vector. For the SDS-PAGE experiments, tandem tagged BTN2A1 and BTN3A1 constructs were used. These were generated using the respective 6xHis tagged templates and the following primers: C-HIS+myc-F, 5' – GGT GGC GGT GGC GAA CAA AAG CTC ATC TCA GAA GAG GAT CTG TGA CTC GAG TCT AGA GGG C – 3'; C-HIS+myc-R, 5' – ATG ATG ATG ATG GTG GTG C – 3'.

ELISA

ELISAs were used to test Vγ9Vδ2 T cell activation by pAg loaded K562 cells with BTN2A1 mutations. Interferon γ (IFNγ) and tumor necrosis factor α (TNFα) secretions were quantified to indicate Vγ9Vδ2 T cell activation. K562 cells depleted of BTN2A1 by CRISPR/Cas9 were transfected with BTN2A1 plasmids with regional mutations or point mutations as generated herein (Figure 2, his-tagged) or described previously (Figure 3, myc-tagged) (17, 20). Transfection was performed by electroporation at 316 volts, 500 mF capacitance and 4 mm conditions. Then, the K562 cells were incubated with pAg POM_2-C-HMBP at 0, 0.1 and 1 μM concentrations for 1 hour. After pAg loading the K562 cells were washed twice, suspended in fresh T cell media and co-cultured with Vγ9Vδ2 T cells in 96 well plates (4,000 K562 cells and 12,000 T cells). 20 hours later, ELISA was performed according to the manufacturer's protocol (Biolegend).

Flow cytometry

BTN2A1 deficient K562 cell line (17) was transiently transfected with BTN2A1 genes with or without mutations in pcDNA3.1 (+) vector or with an empty vector control. All the genes contained an extracellular domain 6x His tag. After 24 hours culture, 2 million cells were washed twice with FACS buffer (2% BSA in PBS), then stained with 3 μL of PE anti-his tag antibody, and fixed with 3% paraformaldehyde. In flow cytometry, cells were gated firstly with FSC and SSC for the major K562 cell population, then percentage of PE positive cells and their mean fluorescence intensity were determined and statistically analyzed.

Western blot and immunoprecipitation

Western blots were used to detect tagged BTN2A1 in BTN2A1 deficient K562 cells following immunoprecipitation. The cells, electroporation conditions, and single tagged myc or his BTN2A1 constructs were previously described (17). Here, cells were co-transfected with 10 μg of each construct (20 μg total) or 20 μg of empty vector (pcDNA3.1(+)) as a negative control. After 24 hours, cells were washed with PBS and lysed using RIPA buffer (25 mM Tris-HCl pH 7.6, 150 mM NaCl, 1% NP-40, 1% sodium deoxycholate, 0.1% SDS) containing the freshly added protease inhibitors aprotinin (1 μg/mL), leupeptin (1 μg/mL), pepstatin (1 μg/mL). Cells were incubated at 4 °C for 15 minutes in RIPA buffer with rotation then centrifuged for 5 minutes at 4°C at 14,000 × g. Supernatants (lysates) were quantified by BCA assay. A portion was reserved for whole cell lysate Western blots.

For immunoprecipitations, 50 μg of protein from each condition was diluted in 500 μL of fresh RIPA buffer with protease inhibitors. The samples were incubated with 3 μL mouse anti-myc-tag antibody for 1 hour with rotation at 4 °C. Then, 30 μL of protein G agarose was added to each tube, and the samples were incubated overnight at 4 °C with rotation. Samples were washed 5 times with 500 μL RIPA and centrifugation for 30 seconds at 2000 × g. To elute the bound protein and separate the BTN2A1 dimer, 30 μL 1X SDS containing dithiothreitol was added to the sample and the tube was then heated for 3 minutes at 95°C with vortexing. The beads were pelleted by centrifugation for 2 minutes at 10,000 × g. Equivalent volumes of 30 μL were loaded onto 10% bis-acrylamide gels. Proteins were transferred to nitrocellulose membranes, blocked with 5% BSA in TBS-T, and blotted with 3 μL of each primary antibody (rabbit anti-myc and mouse anti-his) in 3 mL of blocking buffer. Alexa-Fluor 680 goat-anti-mouse IgG and IRDye 800CW goat-anti-rabbit IgG were used as secondary antibodies at 1:10,000 in TBS-T. Dual color imaging was performed using Licor Odyssey.

Solid-phase peptide synthesis & purification

ELRWRRTFLH-NH_2 was synthesized on Rink Amide resin (0.45 mmol/g loading capacity) using the Syro I automated parallel peptide synthesizer (Biotage). Fmoc-amino acids were coupled twice, using both Oxyma/DIC and HBTU/DIPEA chemistry. The peptide was subsequently cleaved from the resin using a mixture of 95:2.5:2.5 trifluoroacetic acid/ triisopropylsilane/ water. Following ether precipitation and lyophilization, the peptide was purified via reverse-phase high-performance liquid chromatography (RP-HPLC) using a 5% to 95% gradient composed of buffer A (water + 0.1% (v/v) trifluoroacetic acid) and buffer B (acetonitrile + 0.1% (v/v) trifluoroacetic acid). Purity was confirmed with both

RP-HPLC and electrospray ionization mass spectrometry (ESI-MS). The purified peptide was stored as a lyophilized powder. Lyophilized peptide was dissolved and was quantified using absorbance at 280 nm prior to use.

Protein expression and purification

Directional cloning of BTN2A1 and BTN3A1 internal domain constructs into the pET21b vector is described previously (7, 17). Here, the desired point mutations of BTN2A1 were generated using the BTN2A1–271 pET21b or BTN2A1–309 constructs as a PCR template with the following PCR primers. L318G, W320A and L318G/W320A mutations were generated with the common reverse primer 5'- TTG AAG TTT CTC TTT TAC TTG AAG TTC −3' in combination with a forward primer. The forward primers were L318G 5'- GAA GAA GGG CGA TGG AGA AGA ACA TTC TTA CAT −3', W320A GAA GAA TTG CGA GCT AGA AGA ACA TTC TTA CAT GCT GTT −3' or L318G/W320A 5'- GAA GAA GGG CGA GCT AGA AGA ACA TTC TTA CAT GCT GTT −3'. The L325G mutation was generated using the forward primer 5'- AGA ACA TTC GGA CAT GCT GTT GAT GTG GTC CT −3' and the reverse primer 5'- TCT CCA TCG CAA TTC TTC TT −3'. All new point mutations were confirmed by Sanger sequencing.

Plasmids containing the protein of interest were transformed into Rosetta 2 (DE3) pLysS cells for protein expression. For protein expression, bacterial cultures were grown overnight at 37°C and 225 RPM in LB media containing ampicillin and chloramphenicol to be transferred to LB or M9 minimal media. For M9 minimal media, $^{15}NH_4Cl$ was added as the sole nitrogen source. The bacterial cultures were grown at 37°C until the OD_{600} reached approximately 0.5. The culture was transferred to a room temperature shaker and allowed to equilibrate for one hour. The cells were induced by the addition of 1 mM isopropyl β-d-1-thiogalactopyranoside (IPTG) for overnight induction (~18 hours) at room temperature. Bacterial cell pellets were collected and stored at −20°C until needed for further processing.

Protein harvesting was done by resuspending the frozen cell pellets in lysis buffer (50 mM Tris, 200 mM NaCl, 10 mM 2-mercaptoethanol, and 5 mM imidazole, pH 7.4) and then lysing by three passages through a French Press homogenizer (Thermo Fisher Scientific). The cell lysate was centrifuged at 10,000 × g for one hour at 4°C. The supernatant was mixed with Ni-NTA agarose resin (Qiagen) for 45 minutes at 4°C. The resin was washed (50mM Tris, 200 mM NaCl, 10 mM 2-mercaptoethanol, and 20 mM imidazole, pH 7.4) before eluting the protein in elution buffer (50 mM Tris, 200 mM NaCl, 10 mM 2-mercaptoethanol, and 300 mM imidazole, pH 7.4). The elution was further purified by a Superdex 75 16/600 HiLoad Column (GE Healthcare) in the final buffer (50 mM Tris, 100 mM NaCl, 5 mM 2-mercaptoethanol, pH 7.5). The protein fractions were collected and concentrated as needed for subsequent experiments.

Size Exclusion Chromatography

Size exclusion was performed using a Superdex 75 16/600 HiLoad Column (GE Healthcare), where the buffer conditions were 50 mM Tris, 100 mM NaCl, 5 mM 2-mercaptoethanol, pH 7.5. For runs involving BTN2A1 (271–527) or BTN2A1 (309–527) constructs, purified proteins were loaded onto the column at a concentration of 30 μM

with a sample injection volume of 5 mL. For the size exclusion of BTN2A1 (271–527) and BTN3A1 (272–513) mixtures, the proteins were mixed at a concentration of 15 μM BTN3A1 (272–513), 30 μM HMBPP, and/or 30 μM BTN2A1 (271–527) and then incubated overnight at 4°C. Any precipitation was removed by filtering (0.45 μM cellulose acetate filter) prior to loading 5 mL onto the Superdex 75 16/600 column.

Isothermal Titration Calorimetry

ITC was conducted using a low volume nanoITC (TA instruments). The buffer used was 50 mM Tris, 100 mM NaCl, 5 mM 2-mercaptoethanol, pH 7.5. The experimental parameters were 25°C, 20 injections, 2.5 μL per injection, 300 s injection interval, and 200 RPM stirring rate. For experiments titrating in BTN2A1 (271–527) or BTN2A1 (309–527) constructs, the concentration of the titrant was 300 μM and the concentration of the titrand was 60 μM. HMBPP is added to the sample cell at a ratio of 1:2 for BTN3A1 (272–513):HMBPP. When adding in peptide for competitive binding experiments, the peptide ratio (peptide:BTN3A1 (272–513):HMBPP) was 1:1:2, 10:1:2, and 50:1:2. For experiments titrating in peptide, the concentration of the titrant was 700 μM and the concentration of titrand was 100 μM. BTN3A1 (272–513) samples had HMBPP added at a 1:2 ratio. The data was analyzed using NanoAnalyze (TA instruments), where both the regular ITC and competitive ITC data sets were fitted with the independent fit model.

Nuclear Magnetic Resonance

Buffer composition for NMR samples was 50 mM Tris, 100 mM NaCl, 5 mM 2-mercaptoethanol, pH 7.5, and 8% D_2O. Internal reference used was 1 mM 2,2-dimethyl-2-silapentane-5-sulfonic acid (DSS) for DOSY and HSQC experiments. The internal reference for phosphorus NMR was 1 mM inorganic phosphate. For DOSY processing and analysis we utilized VnmrJ; for 2D data - NMRPipe and CcpNmr; and for 1D data - MestreNova, with all the software provided by the NMRbox server (21–23).

^{1}H-^{15}N HSQC experiments were performed on a Varian Inova 600 MHz spectrometer (Agilent Technologies) at 25°C. Spectra were collected using 1024 × 128 increments. Lyophilized peptide was resolubilized in buffer and pH adjusted to 7.5 using NaOH prior to titration experiments at peptide:BTN3A1 (272–513):HMBPP ratios of 5:1:2 and 10:1:2, where the concentration of BTN3A1 (272–513) was 140 μM.

^{1}H-DOSY experiments were performed on a Varian Inova 600 MHz spectrometer (Agilent Technologies) at 25°C. Protein concentration was 400 μM. The DOSY pulse sequence used was DOSY Bipolar Pulse Pair STimulated Echo with Convection Compensation (dbppste_cc). DOSY data sets were collected using 2048 points and 128 scans. Water suppression utilized pre-saturation. The diffusion-encoding pulse strength (gzlvl1) contained an array of 15 randomized values generated by VnmrJ between the minimum and maximum allowed values. Processing was done using VnmrJ. Baseline was corrected by setting integral regions, weighting function was 5 Hz line broadening, and the exponential decay was fitted using the peak heights and two component discrete fit. Fits provided by VnmrJ had an average error of 0.025. The diffusion coefficient was converted to hydrodynamic radius (r) using the equation:

$$D = \frac{RT}{6\pi N r \eta} \quad (1)$$

where R is the ideal gas constant, T is the temperature, N is Avogadro's number, and assuming the viscosity (η) is 0.00091 Pa*s.

^{31}P NMR was performed on a Bruker AVANCE 500 MHz spectrometer (Bruker) with a BBFO smart probe at 25°C. For these experimental series, HMBPP concentration was 100 μM, BTN3A1 (272–513) containing samples were 100 μM, and BTN2A1 (271–527) containing samples were 200 μM. The spectra were collected overnight with 21500 scans using a pulse width of 12.75 μs without decoupling.

Transferred NOESY was obtained of sample containing 2mM peptide with and without BTN3A1 (272–513) at various ratios using a Varian Inova 600 MHz spectrometer (Agilent Technologies) at 25°C. Buffer conditions were 50 mM $NaPO_4$, 100 mM NaCl, 5mM 2-mercaptoethanol, pH 6.0, and 8% D_2O. Data acquisition used 2048 points, 200 increments, 80 scans, 0.3 s mixing time, and pre-saturation for water suppression.

Statistics

The number of independent experiments (n) was listed for each figure. ANOVA was used to calculate significance in bar graphs as indicated. Comparisons were done relative to the control or between pairs of conditions. Columns in bar graphs represent the mean ± standard deviation as indicated in the figure legends. An α level of 0.05 or 0.01 was used as indicated. All statistical analyses were done by GraphPad Prism.

Results

BTN2A1 is a disulfide-linked homodimer, but the disulfide bond is not necessary for pAg detection.

BTN3A1 and BTN2A1 are necessary components of the HMBPP receptor (Figure 1), yet the structures of the complex and their individual components remain unclear. To assess the oligomerization of BTN2A1 and BTN3A1, we expressed these tagged proteins in WT K562 cells and examined them by SDS-PAGE under reducing and non-reducing conditions (Supplemental Figure 1). BTN3A1 ran at similar positions under both reducing and non-reducing conditions. In contrast, BTN2A1 displayed a larger molecular weight under non-reducing conditions. The size difference is consistent with BTN2A1, but not BTN3A1, being a disulfide linked homodimer.

We analyzed the sequence of BTN2A1 and identified two cysteine residues that may contribute to disulfide bond formation (Figure 1). This position is analogous to a similar inter-chain disulfide found in antibody structures. C247 sits just beyond the transmembrane (TM) region on the extracellular side, while C265 is found within the predicted TM region. We generated alanine mutations of each cysteine residue individually as well as in combination. We then tested their ability to enable BTN2A1 deficient K562 cells to stimulate T cell IFNγ production in response to the pAg prodrug POM_2-C-HMBP (7) (Figure 2). As expected, the re-expression of exogenous WT BTN2A1 boosted IFNγ

production relative to the empty vector control, confirming the importance of BTN2A1 for pAg detection in this system. We found that neither cysteine mutant nor the dual cysteine mutant impacted pAg detection (Figure 2A), suggesting that these cysteines and potential disulfides formed by them are not critical to pAg detection. There were no significant changes observed in surface expression of the cysteine mutants, indicating that expression and trafficking of BTN2A1 was also not affected (Figure 2B/C).

Mutations to position 282 do not impact pAg detection.

It was recently discovered that a three amino acid residue sequence within the JM region in BTN3A controls the strength of interaction between various forms of BTN3A dimers, of which there are 6 possible combinations of 3A1, 3A2, and 3A3 (24). BTN2A1 contains an EKE sequence that is associated with strong dimerization (24). To test whether the homologous position is important to dimer formation in BTN2A1, we generated two mutations, BTN2A1 EKE282KKK and EKE282AAA. Our hypothesis was that these mutations might decrease the BTN2A1 homodimer formation or destabilize it through disruption of charge-charge interactions. However, we found that neither mutation impacted pAg detection or surface expression (Figure 2). This suggests that in BTN2A1, unlike BTN3A, charge interactions at this part of the JM region are not necessary for detection of pAgs.

Mutations to BTN2A1 at positions 318 and 325 impact IFNγ and TNFα production by T cells.

It was surprising to us that neither cysteine mutations nor charge mutations impacted pAg response, while previously we had observed that mutations to BTN2A1 between aa316 and aa326 had striking impacts on the ability of Vγ9Vδ2 T cells to produce IFNγ in response to pAgs (17), including at amino acids L318, W320, and L325. To validate and expand these studies, we tested regional and individual point mutations for production of both IFNγ and TNFα at two different pAg concentrations (Figure 3). The regional mutations, mutants 1 and 2, both abrogated pAg response, as did individual mutations L318G and L325G. This was observed at both concentrations of pAg treatment and for expression of both cytokines. However, W320A in this study did not impact the pAg response. Taken together, the two leucine residues in BTN2A1 at positions 318 and 325 are essential for pAg detection, which is abrogated by individual mutation to glycine or alanine mutation in the group.

HMBPP binds BTN3A1 and both phosphates participate in BTN complexes

To further evaluate the contribution of the internal domain of BTN2A1, we purified constructs of BTN2A1 and BTN3A1. We used two different internal constructs of BTN2A1. BTN2A1 (271–527) contains amino acids K271-L527 while BTN2A1 (309–527) contains amino acids Q309-L527. The BTN3A1 full intracellular domain, BTN3A1 (272–513), contains amino acids Q272-A513. Although it is clear that pAgs bind to BTN3A1 and not BTN2A1 (17), we wanted to elucidate whether the two distinct phosphorus atoms of HMBPP behaved differently when bound to BTN3A1. We hypothesized that the terminal phosphate could be exposed to the solvent and be more flexible. This flexibility could be potentially monitored by NMR as the differences in relaxation properties of the two phosphorus atoms, when present, are reflected by variations in the signal to noise ratio and

peaks width when comparing free state to bound state, where each phosphorus could be associated with either BTN3A1 or BTN3A1/BTN2A1 complex.

The HMBPP peaks (Figure 4) were observed at −6.73 ppm and −10.32 ppm, where the peak at −10.32ppm is the α-phosphorus as it shows additional through bond coupling with hydrogen atoms. Control spectra were obtained and are shown in Supplemental Figure 2. The results show that the two phosphorus peaks are broadened beyond detection upon the addition of BTN3A1 (272–513) alone or a mixture of BTN3A1 (272–513):BTN2A1 (271–527) (Figure 4). Since no signal is detected, it is impossible to determine whether the phosphorus atoms experience different environments. On the other hand, the loss of signal is an indicator that there is tight binding between HMBPP and BTN3A1 (272–513) with both phosphorus atoms involved. Additionally, the spectrum of BTN2A1 (271–527):HMBPP gives distinct signals for HMBPP, similar to HMBPP alone, which is in agreement with previous results that showed that BTN2A1 (271–527) does not strongly interact with either phosphate of HMBPP (17). These results demonstrate that HMBPP binds to BTN3A1, but since both phosphorus atoms were broadened beyond detection, additional information about the local environments of the individual phosphorus atoms could not be deduced.

L325G mutation influences BTN2A1 solution dynamics

To further evaluate the influence of amino acids 318, 320, and 325, we generated these point mutations on the BTN2A1 (271–527) and BTN2A1 (309–527) constructs. We collected ^{15}N-HSQC spectra of BTN2A1 (271–527) wild type (WT) and L325G mutant. Unfortunately, the spectral quality of BTN2A1 (271–527) WT was not suitable for further binding studies by chemical shift perturbation as we were only able to detect the random coil regions and side chains (Figure S3E). For comparison, the spectral quality of L325G mutant is very good with chemical shift dispersion and peaks homogeneity resembling a properly folded globular protein of expected molecular weight (30.9 kDa). The reason behind the striking difference between WT and L325G HSQC spectra is the much larger size of the WT hydrodynamic radius, probably due to oligomerization. The only other potential increase in size could be envisioned through a change in conformation between a compact and elongated form, but we doubt that this event could still result in such striking reduction of the spectrum quality. Therefore, we suspect that the WT exists as a dimer while L325G mutant is a monomer. These findings lead us to hypothesize that the L325G mutation disrupts homodimerization of the BTN2A1 internal domain.

To validate the findings that the oligomerization state of BTN2A1 (271–527) was a reason for the low signal to noise, ^{1}H DOSY was obtained for BTN2A1 (271–527) wild type, L318G, W320A, L318GW320A, and L325G. Though there is significant peak overlap, the DOSY results show that there is a consistent difference between L325G compared to all other protein constructs. In Table 1, the averaged diffusion coefficient for L325G hovered around 0.74 (± 0.025) × 10^{-10} m^2/s. In comparison, the averaged diffusion coefficients of the wild type, L318G, W320A, and L318GW320A were closer to 0.65 (± 0.025) × 10^{-10} m^2/s. The DOSY spectra are shown in Supplemental Figure 4. For comparison, 0.74 × 10^{-10} m^2/s and 0.65 × 10^{-10} m^2/s converts to 32.5 Å and 37.1 Å, respectively, using equation 1. Though the signals we are measuring are dominated by side chain moieties, the overall

diffusion rate is still affected by the overall protein size: the observed difference in diffusion coefficients of 1.15 times reflects with the difference in MWs of 1.55 for the simplest spherical model. Thus, we see that there is a significant difference in molecular dynamics when L325 is mutated.

Isolated BTN2A1 internal domains form homodimers

Size exclusion chromatography (Figure 5) corroborates the difference in hydrodynamic radius, where BTN2A1 (271–527) wild type, W320A, and L318GW320A elute at approximately the same volume of 73.5 mL. L318G elutes slightly later at 75.0 mL. L325G elutes at an even later elution volume at 80.4 mL, signifying that L325G has a smaller stokes radius. In terms of molecular weight, our calibration curve (elution volume = −12.67 ln(MW(kDa)) + 122.98) estimated that the molecular weight of L325G is 28.8 kDa compared to 49.6 kDa for the other constructs. Given that the predicted molecular weight of our BTN2A1 (271–527) construct is 30.9 kDa, it is likely that the L325G mutant exists in a monomeric form while the other BTN2A1 (271–527) constructs, including the WT BTN2A1, exist as homodimers.

This data is also consistent when we explored the same L325G mutation on our BTN2A1 (309–527) construct, where the L325G had a longer size exclusion retention time (Figure 5) and a faster diffusion rate (Supplemental Figure 4). Taken together, the internal domain of BTN2A1 has a strong tendency for homodimer formation even in the absence of the TM region and extracellular domains, which is completely disrupted by a single point mutation to L325.

Determining whether a short peptide, containing BTN2A1 residues 318–325, can interact with BTN3A1 or compete with BTN2A1 internal domain, precluding its dimerization

We created a short peptide portion of BTN2A1, containing residues 318–325, so that we could investigate whether or not this small stretch of amino acids is directly involved in BTN2A1 self-association or in interaction with BTN3A1 (Figure 6). We performed ITC by titrating the peptide into the BTN3A1 (272–513):HMBPP complex. Figure 6A shows that the titration heats are close to the control titration, which is an indication of no binding or no detectable heats from binding. Additional titrations performed at 15 °C and 5 °C did not have any significant heats of binding (data not shown). We then tested whether the peptide could interact with BTN2A1 to mimic self-association. First, we tested BTN2A1 (328–527), which is a shorter BTN2A1 construct only contains the B30.2 domain. If the peptide interacts with BTN2A1 (328–527), it could provide insight into the intra-molecular interactions and how the BTN2A1 (271–527) construct may fold back to self-associate with the B30.2 domain. Figure 6B shows that the control and protein titration yielded similar heat values, which indicates that the heats of binding are not detectable or that the peptide does not bind to BTN2A1 (328–527).

A possibility exists that the peptide binds weakly to BTN3A1 (272–513):HMBPP due to the absence of the B30.2 domain of BTN2A1. In the case of weak association, protein concentration limits make it difficult to achieve a proper sigmoidal curve by ITC. To overcome this issue, we conducted competitive binding ITC that would indirectly show if

the peptide binds to BTN3A1 (272–513). The competitive binding ITC experiment (Figure 6C) indicates that BTN2A1 (271–527) can still bind to BTN3A1 (272–513):HMBPP in the presence of peptide. The varying concentration ratios did not influence the K_d or n values (a 0.4 μM to 0.8 μM variation in K_d, when the peptide ratio increased from 1x to 50x, is within the fitting error for the method), whereas there was an apparent change in the enthalpy (Table 2). From this data, we can conclude that the peptide does not bind to BTN3A1 (272–513):HMBPP complex. Because the K_d is practically unaffected, the cause for the discrepancy in the enthalpy is likely the buffer composition as the osmolarity/viscosity increases with the higher concentration of peptide.

BTN2A1 peptide titrations into BTN3A1 (272–513):HMBPP complex were also monitored by ^{15}N-HSQC. As seen in Figure 6D, there are minimal chemical shift perturbations that could be a result from peptide binding. We also tried the transferred NOE approach (25) to see whether this short peptide interacts with BTN3A1 (272–513). Although we saw few additional peaks (an expected manifestation for potential binding), the data was limited (not enough extra peaks to calculate bound conformation for the peptide) and not fully convincing (Supplementary Figure 3A–D). Next, we tested if the peptide could potentially disrupt the BTN2A1 (271–527) dimer. If BTN2A1 (271–527) dimerizes and L325G is a key residue, we hypothesized that adding peptide could lead to new peaks emerging due to improved signal to noise as it was easily seen comparing L325G and wild type BTN2A1 (271–527) (Supplemental Figure 3E). Supplemental figure 3F shows that the additional peptide did not improve the spectral quality, indicating that the solution dynamics of BTN2A1 (271–527) is not significantly altered.

L325G, not L318G or W320A, impacts the formation of BTN3A1:HMBPP:BTN2A1 cytoplasmic complex

A central step in the detection of pAgs is the binding of BTN2A1 to pAg-bound BTN3A1(17). We found that this complex is a stable complex that elutes together in SEC (Figure 5C). Since the protein complex elutes together, it does indicate that the exchange rate for binding is likely in the slow regime, where the bound and unbound states are not readily interconverted. This is further evidenced by NMR titrations (Supplemental Figures 3G and 3H) of BTN2A1 (271–527) into BTN3A1 (272–513) and HMBPP, where we witnessed line broadening accompanied by nearly no chemical shift perturbation, indicating that the bound and unbound states have separate and unique signals. This is more easily visible when examining the shorter BTN3A1 B30.2 only construct (BTN3A1 (340–513)) as we see the unbound state overlaps nicely with the free B30.2. Once the titration ratio increases, the population of bound protein increases and new peaks become visible. This slow exchange of the bound state of the cytoplasmic complex may serve a functional role *in vivo* by keeping the overall protein complex together.

The role of BTN2A1 318–325 in potential binding interactions of the cytoplasmic domains was unclear. To explore the functional relevance of mutations L318G, W320A, and L325G, we performed ITC to determine if these mutations could perturb the binding between BTN3A1:HMBPP and BTN2A1. Figure 7 shows that there are detectable heats of binding when either the WT, L318G mutant or W320A mutant is titrated into BTN3A1 (272–

513):HMBPP complex (Figure 7A, D, E), where the enthalpy of binding is −34.94 ± 4.79 kJ/mol, −39.3 ± 1.1 kJ/mol and −46.0 ± 3.2 kJ/mol, respectively (Table 2). In particular, the K_d values of L318G (1.16 ± 0.24 μM) and W320A (0.67 ± 0.18 μM) are quite similar to the reported binding affinity of wild type BTN2A1 (271–527) (0.886 ± 0.165 μM)(17), suggesting that the mutations did not influence the binding interface. Likewise, the binding affinity of BTN2A1 to BTN3A1:HMBPP is not diminished when EKE282 is mutated to AAA or KKK in our ITC experiments (Figure 7B,C, Table 2).

However, there is a significant difference when L325G mutant is titrated into BTN3A1 (272–513):HMBPP complex as the heat of titration was very similar to the control titration, suggesting that there is no binding. Though another possible explanation is that there is an interaction but no detectable heats of binding, it is highly unlikely that a single L->G mutation can provide enough beneficial changes in entropy to compensate for the loss in enthalpy for binding to occur. This is also supported by the L325G mutation in the shorter BTN2A1 (309–527) construct, which similarly yielded no heats of binding compared to its control (Figure 7H, I). Therefore, the data present strong evidence that the BTN2A1 L325G mutation significantly perturbs the formation the cytoplasmic BTN3A1 (272–513):HMBPP:BTN2A1 (271–527):BTN2A1 (271–527) complex. Lack of a ligand-induced interaction between BTN3A1 and BTN2A1 internal domains caused by the BTN2A1 L325G mutation would likely lead to the loss in cellular pAg response observed in Figure 3.

It was surprising that binding interactions were normal in the L318G, and to a lesser extent, W320A mutants, given their results in cellular functional assays. To rule out that the mutations at 318 and 320 behave as a functional pair, additional ITC experiments were conducted on the double mutant (L318GW320A). Again, the results showed that there was no significant difference as the titration curve and thermodynamic parameters were very similar to the single point mutants L318G and W320A as well as the WT control (Figure 7F, Table 2). Therefore, we suspect that amino acids 318 and 320 do not play a major role in BTN3A1 (272–513):HMBPP:BTN2A1 (271–527) complex formation, and it is possible that L318G impacts cellular function through a different route that is not yet understood or to an extent that cannot be measured by our current methodology.

L325G mutation impacts cellular dimerization of full-length BTN2A1

Because the L325G mutation reduced both the cellular pAg response and the dimerization of the BTN2A1 internal domain, we tested whether or not this mutation would impact cellular dimerization of the full length protein. We co-expressed BTN2A1-myc and 6x his-BTN2A1 in BTN2A1 deficient K562 cells by transient transfection (Figure 8). Expression of both tagged proteins was readily observed by Western blot (Figure 8A), while no bands were observed in cells transfected with empty vectors. In cells expressing both versions of WT BTN2A1, immunoprecipitation with anti-myc tag antibody led to co-immunoprecipitation of his-tagged BTN2A1, as would be expected of this disulfide-linked dimer. The L325G mutation, whether on the myc or his template, reduced the amount of co-immunoprecipitated his-tagged protein (Figure 8B). Together, this data suggests that the

ability of the mutation to block dimerization of the BTN2A1 internal domains also impacts proper formation of the full length cellular dimer.

Discussion

Recent studies have made clear that BTN2A1 and BTN3A1/2/3 work together to sense intracellular pAgs, forming a complex on the cell surface that can be detected by the Vγ9Vδ2 TCR, a new mode of antigen detection in the human immune system. Here, we clarify the role of BTN2A1 homodimerization in this process through examining multiple proposed points of interaction in cellular and biochemical assays.

Clearly, BTN2A1 forms a homodimeric structure. Our findings comparing reducing versus non-reducing conditions are similar to another study (14). Our data show that the BTN2A1 homodimer is disulfide linked, but the disulfide bond is not required for function of the protein. Likewise, our data show that BTN3A1 is not a disulfide-linked dimer. This is consistent with other reports that show 3A1 can form dimeric structures with a second 3A1 molecule, 3A2 or 3A3 (26). These prior studies have found that 3A2, though lacking a pAg binding site, is required for maximal response. The most probable structure of the overall HMBPP receptor is that of a heterotetramer (dimer of dimers) containing two molecules of BTN2A1 as a disulfide linked dimer and one molecule of BTN3A1 in a non-linked dimer with BTN3A2 (or to a lesser extent 3A1 or 3A3) (Figure 1).

In BTN3A proteins, the membrane proximal JM region contains different variations of glutamate and lysine residues, which function to stabilize or destabilize the different possible combinations of BTN3A homodimers (24). In contrast to BTN3A, BTN2A1 contains an EKE sequence. This possibly contributes to a positive homodimeric association in BTN2A1. However, mutation of these residues did not impact the pAg response. Taken together, two likely points of strong interaction in the 2A1 homodimer, C247/C265 and EKE282, tolerated mutation without loss of function, perhaps indicating they show some functional redundancy in stabilizing the BTN2A1 homodimer.

Interestingly, a third point of strong homodimerization within the 2A1 B30.2 domain appears to play a more important role in the pAg response. Single point mutations L318G and L325G abrogate function in cellular assays (Figure 3), consistent with our prior study (17). We have not yet been able to determine the reason for the inconsistency of the W320A mutation, which was functional in this study. Further studies on these internal domain constructs found that BTN2A1 (271–527) and BTN2A1 (309–527) constructs are homodimers even though they lack the disulfide cysteine residues. A stable complex of BTN3A1:HMBPP:BTN2A1 internal domains was also seen by SEC (Figure 5C), but it was not possible to confidently determine specific 3A1:2A1 ratios in this experiment due to protein precipitation as well as potential peak overlap with free 2A1. Though, it is currently assumed to be two molecules of 2A1, one of 3A1, and one of HMBPP. Mutation L325G, but not L318G, resulted both in a strong loss of dimer structure and abrogated binding of BTN2A1 to the ligand bound BTN3A1. Therefore, although L318G does have a clear cellular impact, in the purified proteins it does not affect dimerization, suggesting different mechanisms may cause the cellular phenotypes of L318G and L325G. In BTN3A1,

homodimerization of the B30.2 domain does not seem to be observable by SEC, only in crystal structures (13, 27). Interestingly, the analogous region in BTN3A1 has also been reported to play a role in its function, despite the unclear importance of a 3A1 internal domain homodimer (28) in the context of the 3A1/3A2 dimer being the optimal form. One caveat to these studies is that since our binding assays were done on isolated domain constructs, not the full-length protein. Therefore, we cannot completely rule out the possibility that the internal domain dimer arises from a different pair of BTN2A1 molecules than the two that are disulfide linked. Regardless, our immunoprecipitation experiments do suggest that the L325G mutation negatively impacts cellular dimerization of the full length BTN2A1 protein.

Though the peptide experiments were predominantly negative, some additional peaks in trNOE spectra and small chemical shifts perturbations in HSQC titrations were pointing to the possibility that some non-specific interactions still occurred, though the major portion of the specific binding interface was not formed. A potential problem could be that the peptide stretch did not contain the vital amino acids on either end, which could affect its overall fold, responsible for interacting with 3A1 or 2A1 self-association. Given the role we identified for L325 in BTN2A1 dimerization, it is perhaps surprising that the peptide did not block BTN2A1 dimerization. One possible explanation is that the 2A1 dimerization is characterized by very high affinity or has slow rate of dissociation (K_{off}) so that we were unable to disrupt the interaction by addition of the smaller, not optimized peptide.

Taken together, data presented herein supports the hypothesis that BTN2A1 is a functional homodimer that is maintained by at least three strong points of contact in the linker region (the disulfide bond, the EKE282 region, and the L318–325 region. Surprisingly the most critical region for dimerization that influences the function of the protein is not the disulfide bond or the EKE282 region, but rather the intersection of the JM region with the B30.2 domain, where a single point mutation L325G disrupts 2A1 internal domain dimerization, prevents binding of the 2A1 to the HMBPP bound 3A1, and abrogates cellular dimerization and function.

Supplementary Material

Refer to Web version on PubMed Central for supplementary material.

Acknowledgments

We would like to thank Dr. Vitaliy Gorbatyuk for his assistance with performing NMR experiments, Dr. Heidi Erlandsen for her assistance with the nanoITC, Dr. David Wiemer for providing POM_2-C-HMBP, and Dr. Jin Li for assistance with immunoprecipitation conditions.

This work is financially supported by the National Institute of Health National Institute of Allergy and Infectious Diseases Grant AI150869 (to A.J.W. and O.V.).

References

1. Wiemer AJ 2020. Structure-Activity Relationships of Butyrophilin 3 Ligands. ChemMedChem. 15: 1030–1039. [PubMed: 32453919]

2. Morita CT, Jin C, Sarikonda G, and Wang H 2007. Nonpeptide antigens, presentation mechanisms, and immunological memory of human Vγ9Vδ2 T cells: discriminating friend from foe through the recognition of prenyl pyrophosphate antigens. Immunol. Rev. 215: 59–76. [PubMed: 17291279]

3. Rigau M, Uldrich AP, and Behren A 2021. Targeting butyrophilins for cancer immunotherapy. Trends Immunol. 42: 670–680. [PubMed: 34253468]

4. Gao Z, Bai Y, Lin A, Jiang A, Zhou C, Cheng Q, Liu Z, Chen X, Zhang J, and Luo P 2023. Gamma delta T-cell-based immune checkpoint therapy: attractive candidate for antitumor treatment. Mol. Cancer. 22: 31. [PubMed: 36793048]

5. Harly C, Guillaume Y, Nedellec S, Peigne CM, Monkkonen H, Monkkonen J, Li J, Kuball J, Adams EJ, Netzer S, Dechanet-Merville J, Leger A, Herrmann T, Breathnach R, Olive D, Bonneville M, and Scotet E 2012. Key implication of CD277/butyrophilin-3 (BTN3A) in cellular stress sensing by a major human γδ T-cell subset. Blood. 120: 2269–79. [PubMed: 22767497]

6. Sandstrom A, Peigne CM, Leger A, Crooks JE, Konczak F, Gesnel MC, Breathnach R, Bonneville M, Scotet E, and Adams EJ 2014. The intracellular B30.2 domain of butyrophilin 3A1 binds phosphoantigens to mediate activation of human Vγ9Vδ2 T cells. Immunity. 40: 490–500. [PubMed: 24703779]

7. Hsiao CH, Lin X, Barney RJ, Shippy RR, Li J, Vinogradova O, Wiemer DF, and Wiemer AJ 2014. Synthesis of a phosphoantigen prodrug that potently activates Vγ9Vδ2 T-lymphocytes. Chem. Biol. 21: 945–54. [PubMed: 25065532]

8. Rhodes DA, Chen HC, Price AJ, Keeble AH, Davey MS, James LC, Eberl M, and Trowsdale J 2015. Activation of human γδ T cells by cytosolic interactions of BTN3A1 with soluble phosphoantigens and the cytoskeletal adaptor periplakin. J. Immunol. 194: 2390–8. [PubMed: 25637025]

9. Wang H and Morita CT 2015. Sensor Function for Butyrophilin 3A1 in Prenyl Pyrophosphate Stimulation of Human Vγ9Vδ2 T Cells. J. Immunol. 195: 4583–94. [PubMed: 26475929]

10. Wang H, Nada MH, Tanaka Y, Sakuraba S, and Morita CT 2019. Critical Roles for Coiled-Coil Dimers of Butyrophilin 3A1 in the Sensing of Prenyl Pyrophosphates by Human Vγ9Vδ2 T Cells. J. Immunol. 203: 607–626. [PubMed: 31227581]

11. Nguyen K, Li J, Puthenveetil R, Lin X, Poe MM, Hsiao CC, Vinogradova O, and Wiemer AJ 2017. The butyrophilin 3A1 intracellular domain undergoes a conformational change involving the juxtamembrane region. FASEB J. 31: 4697–4706. [PubMed: 28705810]

12. Gu S, Sachleben JR, Boughter CT, Nawrocka WI, Borowska MT, Tarrasch JT, Skiniotis G, Roux B, and Adams EJ 2017. Phosphoantigen-induced conformational change of butyrophilin 3A1 (BTN3A1) and its implication on Vγ9Vδ2 T cell activation. Proc. Natl. Acad. Sci. U. S. A. 114: E7311–E7320. [PubMed: 28807997]

13. Yang Y, Li L, Yuan L, Zhou X, Duan J, Xiao H, Cai N, Han S, Ma X, Liu W, Chen CC, Wang L, Li X, Chen J, Kang N, Chen J, Shen Z, Malwal SR, Liu W, Shi Y, Oldfield E, Guo RT, and Zhang Y 2019. A Structural Change in Butyrophilin upon Phosphoantigen Binding Underlies Phosphoantigen-Mediated Vγ9Vδ2 T Cell Activation. Immunity. 50: 1043–1053. [PubMed: 30902636]

14. Karunakaran MM, Willcox CR, Salim M, Paletta D, Fichtner AS, Noll A, Starick L, Nohren A, Begley CR, Berwick KA, Chaleil RAG, Pitard V, Dechanet-Merville J, Bates PA, Kimmel B, Knowles TJ, Kunzmann V, Walter L, Jeeves M, Mohammed F, Willcox BE, and Herrmann T 2020. Butyrophilin-2A1 Directly Binds Germline-Encoded Regions of the Vγ9Vδ2 TCR and Is Essential for Phosphoantigen Sensing. Immunity. 52: 487–498. [PubMed: 32155411]

15. Rigau M, Ostrouska S, Fulford TS, Johnson DN, Woods K, Ruan Z, McWilliam HEG, Hudson C, Tutuka C, Wheatley AK, Kent SJ, Villadangos JA, Pal B, Kurts C, Simmonds J, Pelzing M, Nash AD, Hammet A, Verhagen AM, Vairo G, Maraskovsky E, Panousis C, Gherardin NA, Cebon J, Godfrey DI, Behren A, and Uldrich AP 2020. Butyrophilin 2A1 is essential for phosphoantigen reactivity by γδ T cells. Science. 367: eaay5516. [PubMed: 31919129]

16. Cano CE, Pasero C, De Gassart A, Kerneur C, Gabriac M, Fullana M, Granarolo E, Hoet R, Scotet E, Rafia C, Herrmann T, Imbert C, Gorvel L, Vey N, Briantais A, le Floch AC, and Olive D 2021. BTN2A1, an immune checkpoint targeting Vγ9Vδ2 T cell cytotoxicity against malignant cells. Cell Rep. 36: 109359. [PubMed: 34260935]

17. Hsiao CC, Nguyen K, Jin Y, Vinogradova O, and Wiemer AJ 2022. Ligand-induced interactions between butyrophilin 2A1 and 3A1 internal domains in the HMBPP receptor complex. Cell Chem Biol. 29: 985–995 e5. [PubMed: 35081362]

18. Willcox CR, Salim M, Begley CR, Karunakaran MM, Easton EJ, von Klopotek C, Berwick KA, Herrmann T, Mohammed F, Jeeves M, and Willcox BE 2023. Phosphoantigen sensing combines TCR-dependent recognition of the BTN3A IgV domain and germline interaction with BTN2A1. Cell Rep. 42: 112321. [PubMed: 36995939]

19. Kilcollins AM, Li J, Hsiao CH, and Wiemer AJ 2016. HMBPP Analog Prodrugs Bypass Energy-Dependent Uptake To Promote Efficient BTN3A1-Mediated Malignant Cell Lysis by Vγ9Vδ2 T Lymphocyte Effectors. J. Immunol. 197: 419–28. [PubMed: 27271567]

20. Hsiao CC and Wiemer AJ 2022. Generation of effector Vγ9Vδ2 T cells and evaluation of their response to phosphoantigen-loaded cells. STAR Protoc. 3: 101422. [PubMed: 35677612]

21. Delaglio F, Grzesiek S, Vuister GW, Zhu G, Pfeifer J, and Bax A 1995. NMRPipe: a multidimensional spectral processing system based on UNIX pipes. J. Biomol. NMR. 6: 277–93. [PubMed: 8520220]

22. Maciejewski MW, Schuyler AD, Gryk MR, Moraru II, Romero PR, Ulrich EL, Eghbalnia HR, Livny M, Delaglio F, and Hoch JC 2017. NMRbox: A Resource for Biomolecular NMR Computation. Biophys. J. 112: 1529–1534. [PubMed: 28445744]

23. Vranken WF, Boucher W, Stevens TJ, Fogh RH, Pajon A, Llinas M, Ulrich EL, Markley JL, Ionides J, and Laue ED 2005. The CCPN data model for NMR spectroscopy: development of a software pipeline. Proteins. 59: 687–96. [PubMed: 15815974]

24. Karunakaran MM, Subramanian H, Jin Y, Mohammed F, Kimmel B, Juraske C, Starick L, Nöhren A, Länder N, Willcox CR, Singh R, Schamel WW, Nikolaev VO, Kunzmann V, Wiemer AJ, Willcox BE, and Herrmann T 2023. Division of labor and cooperation between different butyrophilin proteins controls phosphoantigen-mediated activation of human γδ T cells. Research square.

25. Vinogradova O and Qin J 2012. NMR as a unique tool in assessment and complex determination of weak protein-protein interactions. Top. Curr. Chem. 326: 35–45. [PubMed: 21809187]

26. Vantourout P, Laing A, Woodward MJ, Zlatareva I, Apolonia L, Jones AW, Snijders AP, Malim MH, and Hayday AC 2018. Heteromeric interactions regulate butyrophilin (BTN) and BTN-like molecules governing γδ T cell biology. Proc. Natl. Acad. Sci. U. S. A. 115: 1039–1044. [PubMed: 29339503]

27. Gu S, Borowska MT, Boughter CT, and Adams EJ 2018. Butyrophilin3A proteins and Vγ9Vδ2 T cell activation. Semin. Cell Dev. Biol. 84: 65–74. [PubMed: 29471037]

28. Peigne CM, Leger A, Gesnel MC, Konczak F, Olive D, Bonneville M, Breathnach R, and Scotet E 2017. The Juxtamembrane Domain of Butyrophilin BTN3A1 Controls Phosphoantigen-Mediated Activation of Human Vγ9Vδ2 T Cells. J. Immunol. 198: 4228–4234. [PubMed: 28461569]

Key Points

- Mutations to BTN2A1 L318 and L325, but not C247, C265, or EKE282, block pAg response
- BTN2A1 cytoplasmic domain is a stable dimer that interacts with HMBPP-bound BTN3A1
- L325G mutation disrupts BTN2A1 dynamics, dimerization, and affinity to BTN3A1:HMBPP

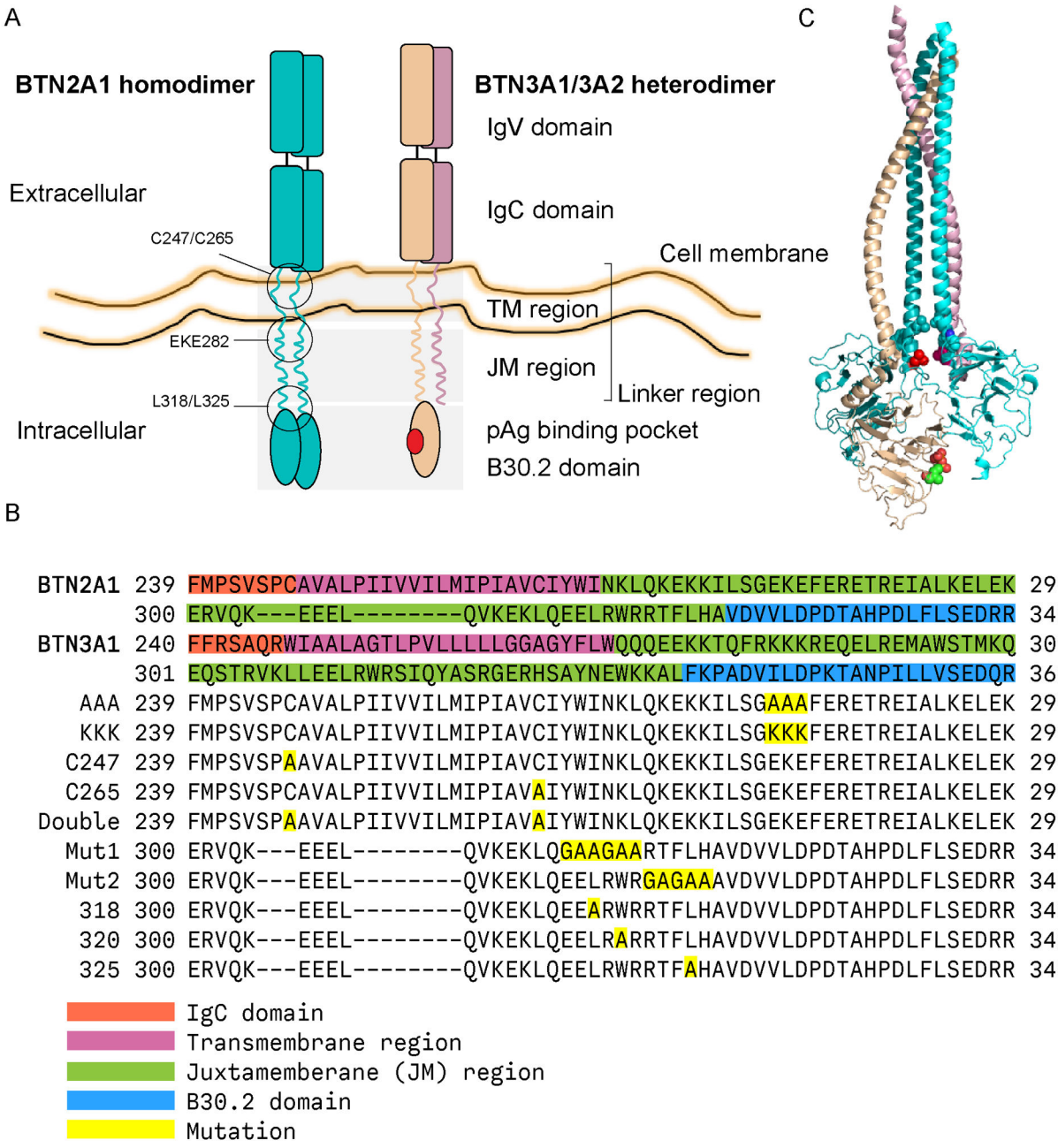

Figure 1.

Diagrams of BTN2A1 and BTN3A1 structures and relevant sequences. (A) Diagram of BTN2A1 and BTN3A1 showing that each monomer has one IgV domain, one IgC domain, one TM region, one JM region and one B30.2 domain. The pAg binding site is in the BTN3A1 B30.2 domain. A B30.2 domain is not found in BTN3A2. We refer to the region connecting the IgC and the B30.2 domains of BTN2A1 as the linker region in this paper. (B) Mutations to BTN2A1 used in this paper were AAA (EKE282AAA), KKK (EKE282KKK), cysteine point mutation C247 (C247A), cysteine

point mutation C265 (C265A), double cysteine point mutation (C247A and C265A), mutation 1 (EELRWR316GAAGAA), mutation 2 (RTFLH322GAGAA), point mutation 318 (L318A), point mutation 320 (W320A) and point mutation 325 (L325A). The different regions of BTN2A1 and BTN3A1 protein sequences are shown in different colors. (C) A structural model of assembled complex. BTN2A1 is shown in blue, while BTN3A1 is in yellow. L325 is highlighted in red at the intersection of the JM and B30.2 domain. The pAg is shown in green. Other mutated residues are thought to be on the internal facing side of the BTN2A1 alpha helixes.

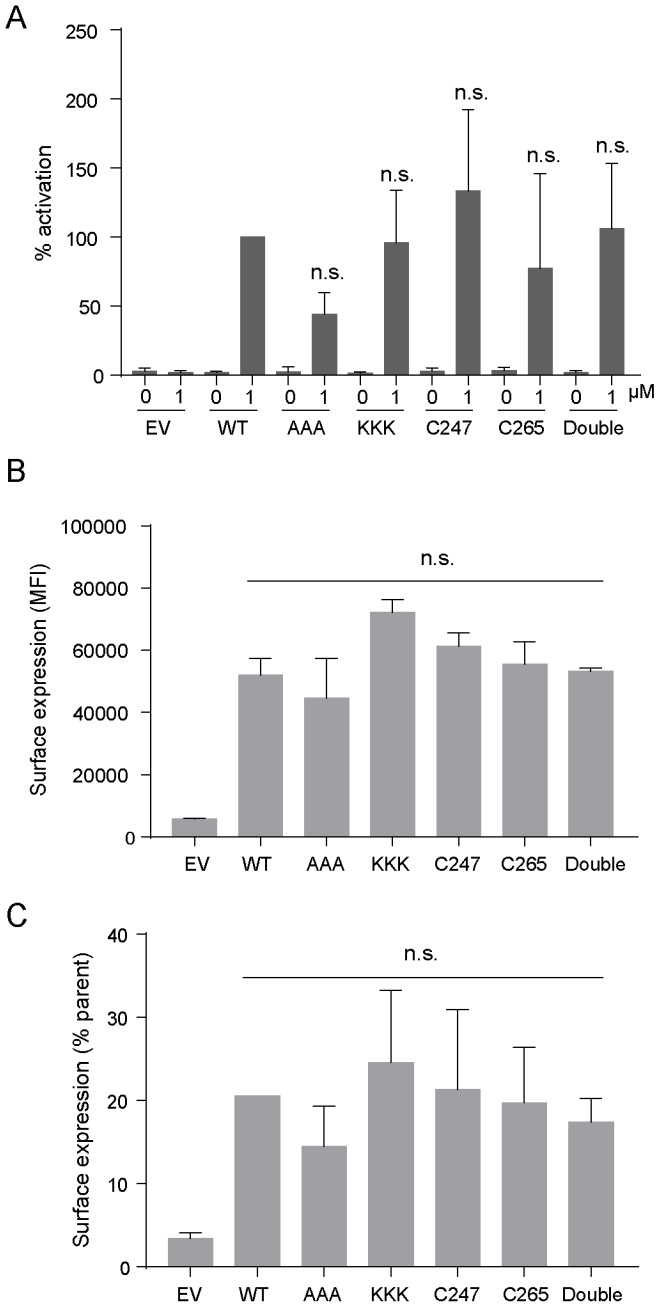

Figure 2.

BTN2A1 C247, C265 and EKE282 are not required for pAg detection. (A) BTN2A1 deficient K562 cells were transfected with plasmids of empty vector (EV), wild type his-tagged BTN2A1 (WT), JM region mutation AAA (EKE298AAA), JM region mutation KKK (EKE298KKK), extracellular cysteine point mutation C247 (C247A), TM cysteine point mutation C265 (C265A) and double cysteine point mutation (C247A and C265A). Then Vγ9Vδ2 T cells were co-cultured with K562 cells pre-loaded with pAg prodrug POM_2-C-HMBP concentrations of 0 and 1 μM for 1 hour. Vγ9Vδ2 T cell activation was

tested and indicated by IFNγ secretion through ELISA. The response of the WT BTN2A1 was set to 100%. (B and C) K562 cells expressing BTN2A1 with indicated mutations were tested by flow cytometry after staining with His-tag antibody to verify the mutated BTN2A1 protein surface expression levels. Mean fluorescence intensity (MFI) and BTN2A1 expression positive cell percentages are shown. Statistical significance was determined by one-way ANOVA with Dunnett analysis. n.s. means no significant difference. Columns represent the mean ± stdev. n = 4 replicates. Vγ9Vδ2 T cells were from at least two donors.

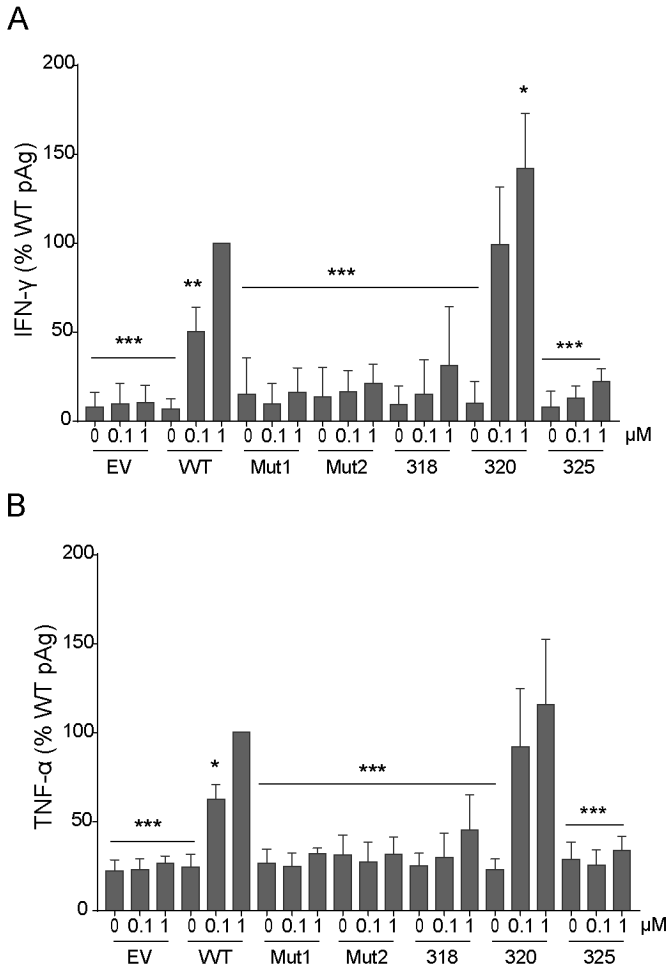

Figure 3.

Mutations to the BTN2A1 internal domain affect Vγ9Vδ2 T cell pAg response. BTN2A1 deficient K562 cells were transfected with plasmids of empty vector (EV), wild type myc-tagged BTN2A1 internal domain (WT), regional mutation 1 (Mut1, EELRWR316GAAGAA), regional mutation 2 (Mut2, RTFLH322GAGAA), point mutation on the 318 amino acid (318, L318G), point mutation on 320 amino acid (320, W320A) and point mutation on 325 amino acid (325, L325G). Then Vγ9Vδ2 T cells were co-cultured with K562 cells loading pAg of 0, 0.1 and 1 μM for 1 hour. Vγ9Vδ2 T cell activation was tested and indicated by IFNγ (A) and TNFα (B). Statistical significance was determined by one-way ANOVA with Dunnett analysis. *p<0.05, **p < 0.01 and ***p<0.001 versus WT 1 concentration pAg treated control. Columns represent the mean ± stdev. n = 3 replicates. Vγ9Vδ2 T cells were from at least two donors.

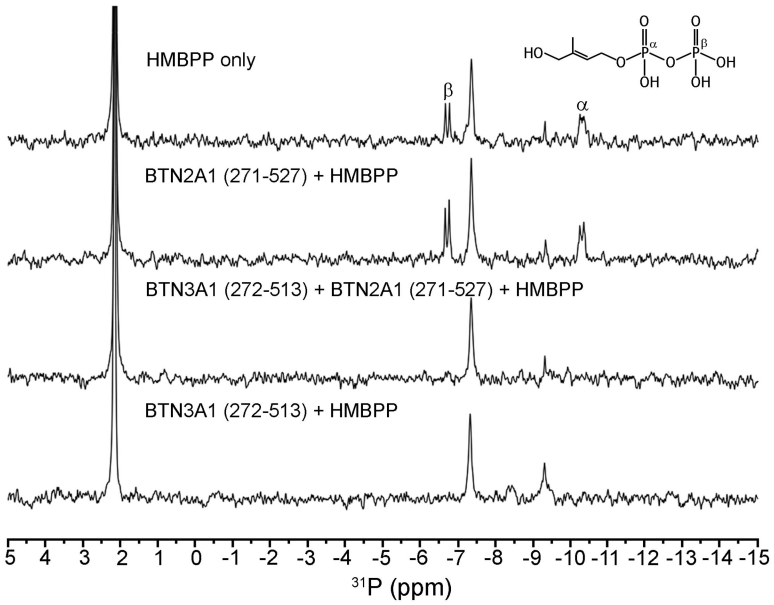

Figure 4.

^{31}P spectra showing the observed peaks from various samples (labeled above). The peak at 2.15 ppm is inorganic phosphate. The two doublets (−6.73 ppm and −10.32 ppm) correspond to the two HMBPP phosphorus atoms (labeled on the molecular structure). The doublet at −10.32ppm is the α-phosphorus as it shows through bond coupling with hydrogen atoms. The singlet at −7.38 ppm is likely to be pyrophosphate, a contaminant. The singlet seen at −9.33 ppm is unknown.

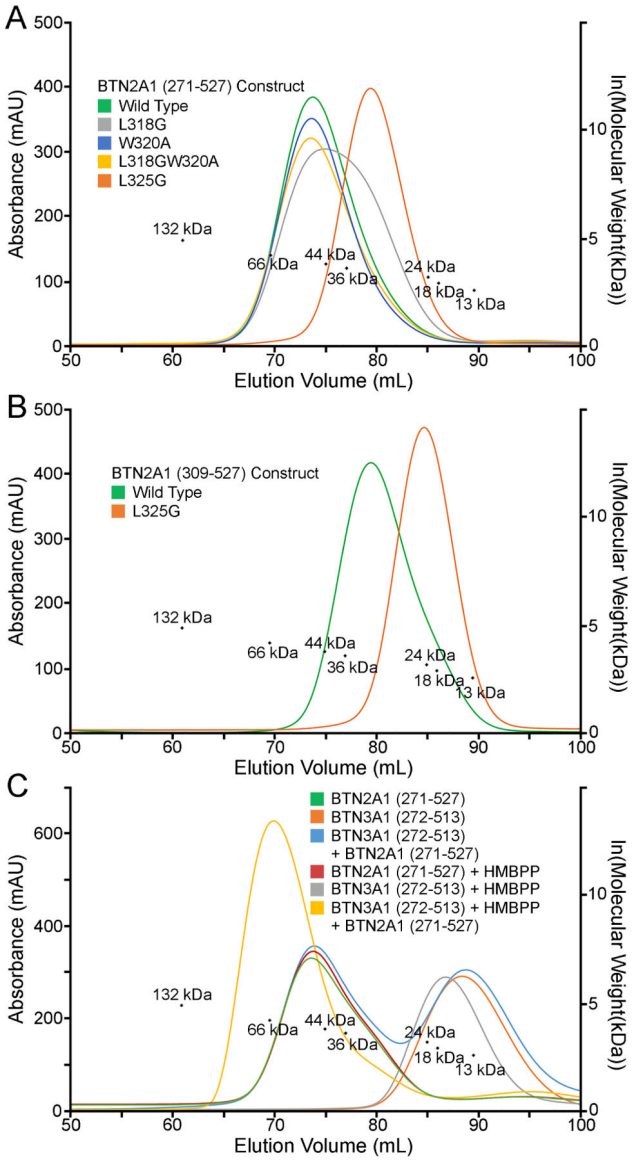

Figure 5.

Size exclusion chromatography elution profiles overlaid with the molecular weight markers of (A) BTN2A1 (271–527) constructs, (B) BTN2A1 (309–527) constructs, or (C) various mixtures of BTN2A1 (271–527) and BTN3A1 (272–513) are shown. For (A), sample injections were 5 mL with 30 μM protein concentration. The elution volume of wild type is 73.7 mL, L318G is 75.0 mL, L318GW320A is 73.5 mL, W320A is 73.5 mL, and L325G is 80.4 mL. For (B), sample injections were 5 mL with 30 μM protein concentration. The elution volume of wild type is 79.5 mL and L325G is 84.7 mL. For (C), sample injection volume was 5 mL. Concentrations of protein were 30 μM BTN2A1 (271–527), 30 μM HMBPP, and/or 15 μM BTN3A1 (272–513). The elution volumes of BTN2A1 (271–527) only is 73.7 mL, BTN3A1 (272–513) only is 88.3 mL, BTN3A1 (272–513) with HMBPP is 86.9 mL, and BTN3A1 (272–513) with BTN2A1 (271–527) and HMBPP is 70.3 mL.

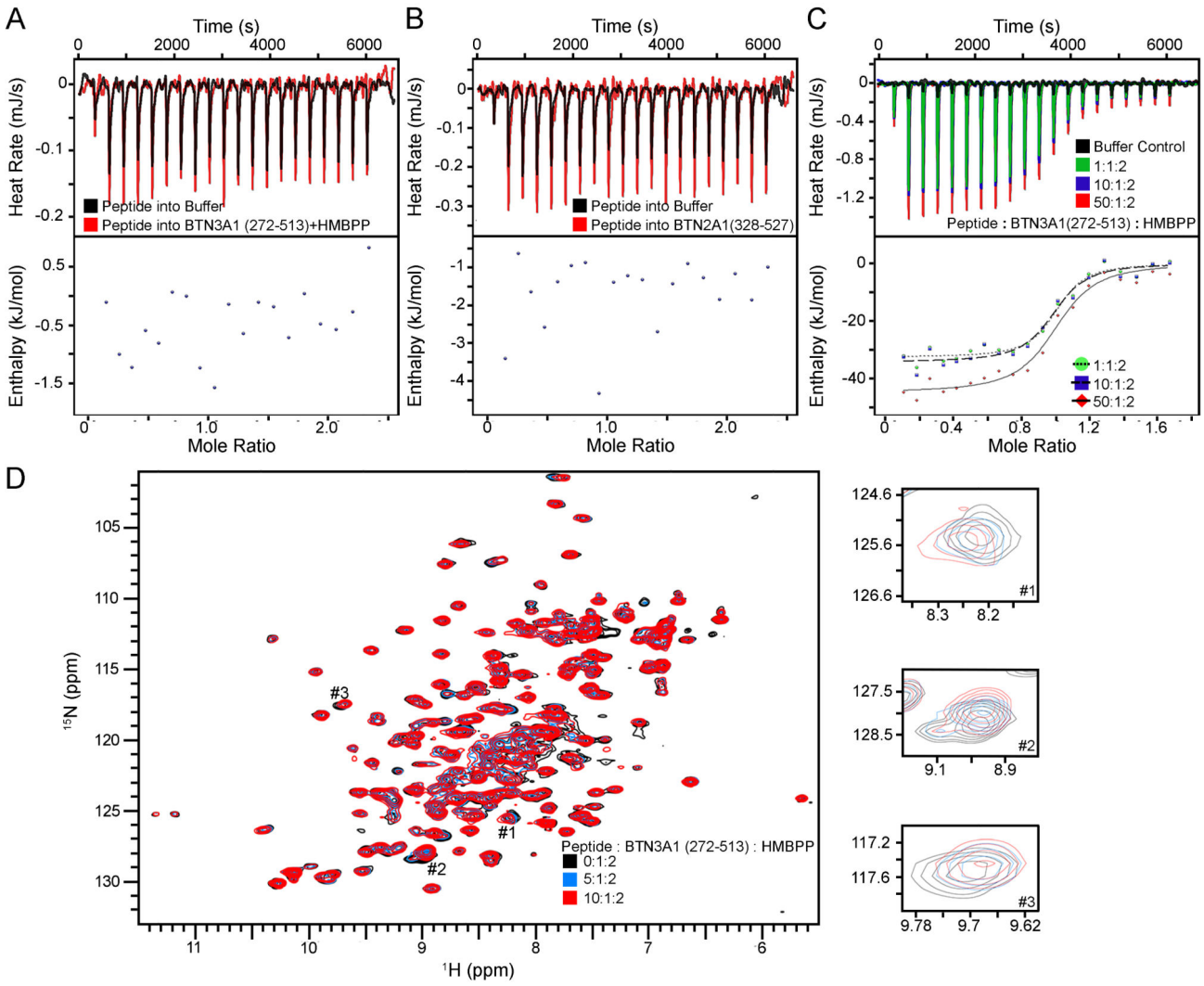

Figure 6.

ITC binding experiments with the peptide are shown. For direct binding experiments, 700 μM peptide was titrated into (A) 100 μM BTN3A1 (272–513) and 200 μM HMBPP or (B) 100 μM BTN2A1 (328–527). (C) Individual ITC thermograms for competitive binding ITC are shown, where 300 μM BTN2A1 (271–527) is titrated into a solution containing 60 μM BTN3A1 (272–513) and 120 μM HMBPP with various concentration ratios of peptide. The corrected heats and fits are visualized in the bottom box. (D) ^{1}H-^{15}N HSQC overlay of peptide titration experiments. BTN3A1 (272–513):HMBPP ratio is 1:2. The small changes in chemical shift for three different peaks (labeled by number in the full spectrum) are more clearly shown on the right hand side.

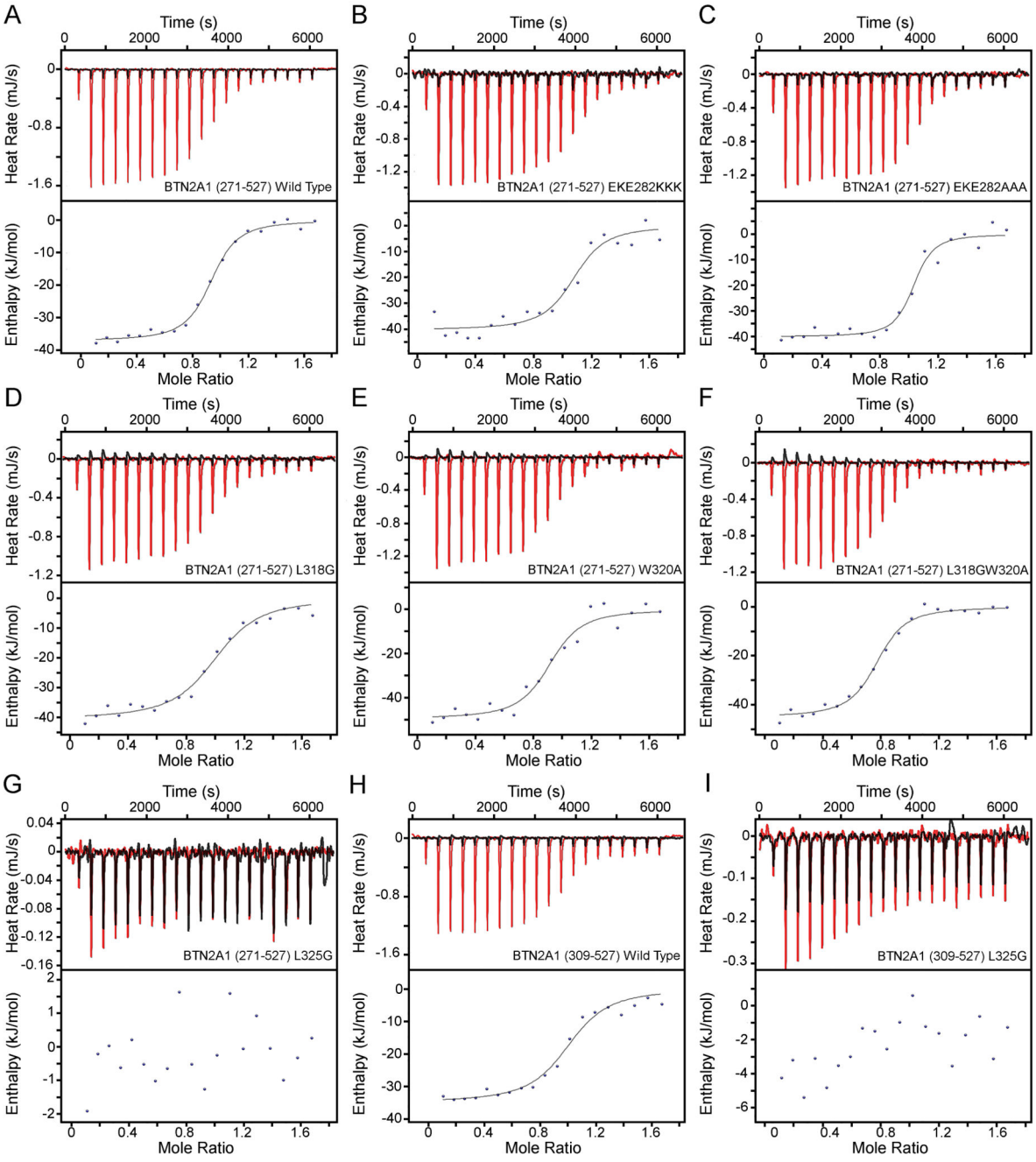

Figure 7.

ITC experiments of BTN2A1 mutants titrated into BTN3A1 (272–513):HMBPP. All samples had a titrant concentration of 300 μM. The titrand was BTN3A1 (272–513):HMBPP at 60 μM and 120 μM, respectively. Control titrations into buffer are shown in black and protein titration runs are shown in red. The corrected heats of binding are shown in the bottom box, where the independent fit model is shown if a good fit was obtained. The titrations using BTN2A1 (271–517) constructs are (A) Wild type, (B) EKE282KKK, (C)

EKE282AAA, (D) L318G, (E) W320A, (F) L318GW320A, and (G) L325G. The titrations using BTN2A1 (309–517) constructs are (H) Wild type and (I) L325G.

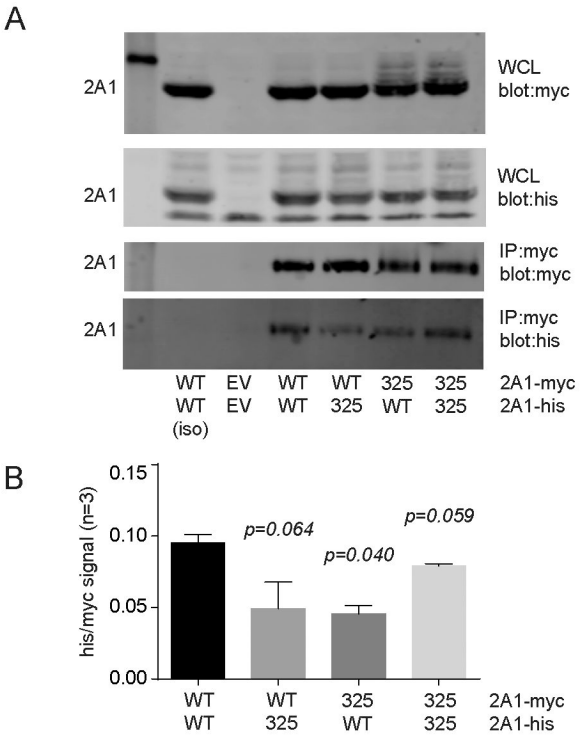

Figure 8.

L325G mutation disrupts co-immunoprecipitation of myc- and his- tagged BTN2A1.

(A) BTN2A1 deficient K562 cells expressing myc-tagged and his-tagged BTN2A1 were assessed by Western blot. Top, whole cell lysate (WCL) blots for myc or his tag. No band is observed in empty vector (EV) controls. Bottom, myc immunoprecipitations blotted for myc or his tag. No bands are observed in isotype (iso) control or EV control. (B) Quantification of the his signal as a percentage of the myc signal. Statistical significance was determined by one-way ANOVA with Tukey's analysis. The p values are indicated relative to WT/WT control. Columns represent the mean ± stdev. n = 3 replicates.

Table 1.

Diffusion Coefficients of BTN2A1 (271–527) Mutants

BTN2A1 (271–527) Construct	Averaged Aliphatic Diffusion (x 10^{-10} m^2/s)	Averaged Amide Diffusion (x 10^{-10} m^2/s)
Wild Type	0.679	0.624
L318G	0.662	0.666
W320A	0.571	0.682
L318GW320A	0.634	0.680
L325G	0.745	0.742

Averaged diffusion coefficients of different BTN2A1 (271–527) constructs are given. Aliphatics grouped together coefficients between 0.6 ppm and 2.7 ppm while amides grouped together coefficients between 6.7 ppm to 8.0 ppm. Diffusion coefficients that were greater than 2 were not included in the averaging.

Table 2.

Thermodynamic Binding Parameters of 2A1 Titrations into 3A1 mixtures

Titrand	Titrant	Kd (μM)	N	ΔH (kJ/mol)	ΔS (J/mol*K)
BTN3A1 (272–513):HMBPP (1:2)	BTN2A1 (271–527) Wild Type (from Hsiao 2022)	0.89 + 0.17	0.74 ± 0.12	−34.9 ± 4.8	−1.2
	BTN2A1 (271–527) L318G	1.16 ± 0.24	1.14 ± 0.16	−39.3 ± 1.1	−18.3 ± 4.4
	BTN2A1 (271–527) W320A	0.67 ± 0.18	0.98 ± 0.11	−46.0 ± 3.2	−36.1 ± 12.3
	BTN2A1 (271–527) L318GW320A	0.71 ± 0.02	0.76 ± 0.02	−45.1 ± 0.3	−33.7 ± 0.7
	BTN2A1 (271–527) EKE282KKK	0.61	1.048	−40.3	−16.4
	BTN2A1 (271–527) EKE282AAA	2.43	0.989	−39.9	−7.4
Peptide: BTN3A1 (272–513):HMBPP (1:1:2)	BTN2A1 (271–527) Wild Type	0.41	0.97	−32.6	12.8
Peptide: BTN3A1 (272–513):HMBPP (10:1:2)	BTN2A1 (271–527) Wild Type	0.55	0.96	−34.3	4.8
Peptide: BTN3A1 (272–513):HMBPP (50:1:2)	BTN2A1 (271–527) Wild Type	0.81	0.98	−44.8	−33.7

ITC thermodynamic parameters from independent fit model. The number of repetitions for the experiments are 3 for L318G, W320A, 2 for L318GW320A, 1 for peptide binding, 1 for EKE mutants. The standard deviation is given for runs with 2 or more attempts.